Adsorption (2014) 20:53–60
DOI 10.1007/s10450-013-9548-x

Numerical simulation of rapid pressurization and depressurization of a zeolite column using nitrogen

Vemula Rama Rao · Mayuresh V. Kothare · Shivaji Sircar

Received: 15 January 2013 / Accepted: 25 April 2013 / Published online: 9 May 2013

Abstract The required durations of pressurization and depressurization steps of a rapid pressure swing adsorption process are primarily governed by adsorbent particle size, adsorption kinetics, column pressure drop, column length to diameter ratio, and the valve constant of the gas inlet and outlet control valve attached to the adsorbent column. A numerical model study of the influence of these variables for an adiabatic LiX zeolite column is presented using pure N_2 as an adsorbate gas. An adsorbent particle size range of 200–350 μm was found to minimize (<1 s) the times required for the pressurization and depressurization steps.

Keywords Rapid depressurization · Rapid pressurization · Zeolite column · Nitrogen · Mathematical simulation · LiX zeolite

1 Introduction

Rapid pressure swing adsorption (RPSA) process cycles are frequently used in the design of medical oxygen concentrators (MOC) for production of 90+ % O_2 from ambient air employing LiX zeolite as the nitrogen selective adsorbent and a Skarstrom—like PSA cycle consisting of ad(de)sorption steps such as (a) column pressurization to a super-atmospheric pressure level with feed air or product gas or a combination of the two, and (b) high pressure adsorption from feed air to produce the oxygen enriched product gas, followed by counter-current desorption steps such as (c) column depressurization to ambient pressure, and (d) back purge with a part of the product gas. A recent experimental study indicated that the total cycle time (t_c) of such a RPSA process cannot be reduced indefinitely in order to increase the cycling frequency, and hence reduce the bed size factor (BSF: amount of adsorbent per unit product withdrawal rate) of the process design due to finite mass, heat and momentum transfer resistances encountered by a real adsorption process. It was found that a minimum in BSF can be achieved by using a t_c of 3–5 s while using an adsorption pressure of 2–4 atm (Chai et al. 2011). A BSF of <60 *lbs/TPD* (*ton per day*) of contained O_2 can be achieved.

Consequently, the allowable cycle times for the individual steps of an optimized four-step RPSA process are limited, being in the order of <1 s and preferably <0.5 s. We recently carried out several numerical evaluations of the efficiency of N_2 desorption from a LiX zeolite column using a rapid O_2 purge [equivalent to step (d) of the RPSA scheme] and found that, ad(de)sorption kinetics, column non-isothermality and pressure drop play important roles in lowering the efficiency of desorption by rapid O_2 purge while the gas phase mass axial dispersion and a finite gas–solid heat transfer coefficient have little effect on the desorption efficiency (Chai et al. 2012, 2013). The studies showed that an optimum adsorbent particle diameter of 300–500 μm facilitates efficient desorption by product O_2 back purge. A pancake adsorber design lowers the negative effect of column pressure drop during desorption by purge, but reduces the length of the N_2 free zone at the purge inlet end (Chai et al. 2013).

The objective of the present work is to numerically investigate the effects of the above mentioned transport resistances in determining the durations of rapid pressurization and depressurization processes [steps (a) and (c)] for an adiabatic LiX zeolite column using pure N_2 as the adsorbate gas.

V. R. Rao · M. V. Kothare · S. Sircar (✉)
Department of Chemical Engineering, Lehigh University, Bethlehem, PA 18015, USA
e-mail: sircar@aol.com

Figure 1 is a schematic drawing of the pressurization–depressurization scheme studied in this work. Pure N_2 at pressure P^0 and temperature T^0 is introduced into an adiabatic column packed with LiX zeolite particles through a flow control valve having a valve constant of C_v. The adsorbent is initially equilibrated with N_2 at ambient pressure (P_{atm}) and T^0. The column gas phase pressure at the end of the pressurization process is P^0 and the adsorbent temperature is T^* ($>T^0$) due to evolution of heat of adsorption. The column is then depressurized through the same valve from P^0 to P_{atm} when the adsorbent temperature changes from T^* to T^{**}. The inlet and exit gas flow rates during these steps can be changed by altering the valve constant (C_v). A larger value of C_v translates to a larger valve opening. The open and closed ends of the column are designated by $z = L$ and $z = 0$, respectively, where $0 \le z \le L$ is the distance in the column. The length of the column is L and its diameter is D.

2 Mathematical model

The mathematical model for numerical simulation of rapid pressurization of an adiabatic LiX zeolite column with N_2 followed by N_2 desorption by rapid column pressure reduction was formulated by a set of partial differential equations (PDE) which describe (a) transient gas and adsorbed phase mass balances for N_2, (b) gas and solid phase energy balances, and (c) column pressure drop. They are given below [Eq. (1–5)]:

Gas phase mass balance for N_2:

$$\varepsilon \frac{\partial}{\partial}\left[\rho_g\right] = -\frac{\partial}{\partial z}[Q] - \rho_b \frac{\partial n}{\partial t} + \bar{\varepsilon} D_L \frac{\partial^2}{\partial z^2}\left[\rho_g\right] \tag{1}$$

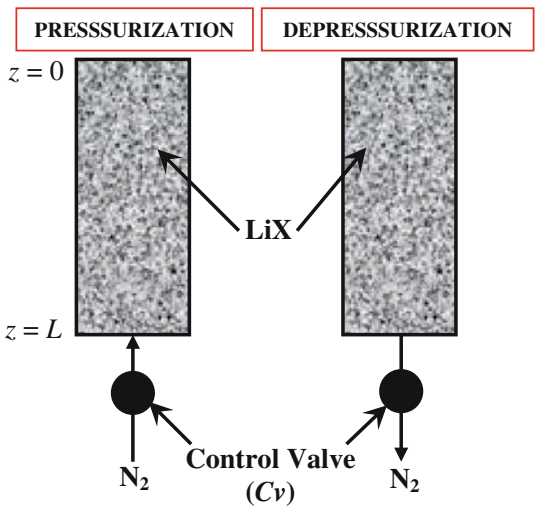

Fig. 1 Schematic drawing of pressurization–depressurization model

Adsorbed phase mass balance for N_2 (LDF model):

$$\frac{\partial n}{\partial t} = k[n^{\infty} - n] \tag{2}$$

Gas phase heat balance:

$$\varepsilon C_g \frac{\partial}{\partial t}\left[\rho_g \theta_g\right] = -C_g \frac{\partial}{\partial z}\left[Q\theta_g\right] + ha\left(T_s - T_g\right) + \bar{\varepsilon} C_g D_g \frac{\partial^2}{\partial z^2}\left[\rho_g \theta_g\right] \theta_g(z,\ t) = \left(T_g - T_0\right) \tag{3}$$

Solid phase heat balance:

$$\rho_b C_s \frac{\partial}{\partial t}[\theta_s] = \rho_b \sum q \frac{\partial n}{\partial t} - ha\left(T_s - T_g\right) \qquad \theta_s(z,\ t) = \left(T_s - T_g\right) \tag{4}$$

Column pressure drop (Ergun 1952):

$$\left(\frac{\partial P}{\partial z}\right)_t = -\frac{150\mu_g}{d_p^2 \rho_g}\frac{(1-\bar{\varepsilon})^2}{\bar{\varepsilon}^3} Q - \frac{1.75 M_g}{d_p \rho_g}\frac{(1-\bar{\varepsilon})}{\bar{\varepsilon}^3} Q^2 \tag{5}$$

where $n\,(z, t)$ is the specific amount of N_2 adsorbed at distance $z(0 \le z \le L)$ in the adsorbent column at time t. $n^{\infty}(z, t)$ is the equilibrium amount of N_2 adsorbed under the local gas phase conditions at z and t. The parameters $Q(z, t)$, $P(z, t)$ and $\rho_g(z, t)\left[= P/RT_g\right]$ are, respectively, the gas phase mass flux [based on empty cross section area $A(= \pi D^2/4)$, of the adsorber], gas pressure, and gas density at z and t. It is assumed that the gas phase is ideal. The variables $T_s(z, t)$ and $T_g(z, t)$ are, respectively, the solid and gas phase temperatures at z and t. The initial column temperature is T^0. The parameter k is the linear driving force (LDF) mass transfer coefficient for N_2. The variable h is the gas–solid heat transfer coefficient, and $a\left[= 6(1-\bar{\varepsilon})/d_p\right]$ is the effective surface area per unit column volume for gas–solid heat transfer. The variables D_L and $D_g\left[= k_g/\rho_g C_g\right]$ are, respectively, the gas phase effective axial mass and heat dispersion coefficients. k_g, μ_g, C_g and M_g are, respectively, the gas phase thermal conductivity, viscosity, heat capacity, and molecular weight. The parameters ε, $\bar{\varepsilon}$, ρ_b, and d_p are, respectively, the helium void fraction, interparticle void fraction, adsorbent bulk density, and adsorbent particle diameter in the column. R is the gas constant.

The key features of the proposed model are (a) inclusion of a finite adsorbate mass transfer resistance, (b) inclusion of axial mass and heat dispersion in the gas phase, (c) inclusion of gas–solid heat transfer resistance, (d) exclusion of axial conduction of heat in the solid phase, and (e) inclusion of transient pressure drop in the gas phase by employing a differential form of Ergun equation to describe local pressure drop in the column. Other important model assumptions are (a) adiabatic column behavior, (b) absence of radial gradients inside the column, and

(c) absence of gas mal-distribution or particle agglomeration.

The initial and boundary conditions used for numerical solutions of the above described model equations are summarized below. They have been traditionally used by various authors:

Initial conditions:

Pressurization:

$$P(z,0) = P_{atm}; \quad T_g(z,0) = T_s(z,0) = T^0 \tag{6}$$

Depressurization:

$$P(z,0) = P^0; \quad T_g(z,0) = T_s(z,0) = T^* \tag{7}$$

Boundary conditions:

Column closed end (z = 0) at all time:

Pressurization and Depressurization (Danckwerts 1953):

$$\frac{\partial P}{\partial z} = 0 \tag{8}$$

$$\frac{\partial}{\partial z}\left[\rho_g \theta_g\right] = 0 \tag{9}$$

The gas flow rate at the closed end is given by:

$$Q(0,t) = 0 \tag{10}$$

Column open end (z = L) at all time:

Pressurization (Teague and Edgar 1999; Jee et al. 2001, 2005; Nikolic et al. 2008):

$$\bar{\varepsilon} D_g \frac{\partial}{\partial z}\left[\rho_g \theta_g\right] = -Q(L,t)\left[\theta_g\big|_{z=L^+} - \theta_g\big|_{z=L^-}\right] \tag{11}$$

Depressurization (Schiesser 1996; Chai et al. 2012):

$$\varepsilon C_g \frac{\partial}{\partial t}\left[\rho_g \theta_g\right] = -C_g \frac{\partial}{\partial z}\left[Q\theta_g\right] + ha\left(T_s - T_g\right) \tag{12}$$

The gas flow rate at the open end is given by (Santos et al. 2007):

$$\begin{aligned} Q(L,t) = & -A\Delta P^6 + B\Delta P^5 - C\Delta P^4 \\ & + D\Delta P^3 - E\Delta P^2 + F\Delta P \end{aligned} \tag{13}$$

where $\Delta P = [P^0 - P(L,t)]$ for pressurization, and $\Delta P = [P(L,t) - P_{atm}]$ for depressurization.

Equation (13) empirically describes the flow rate through the control valve of Fig. 1 for a given pressure gradient (ΔP) across it. The constants A–F in the equation are empirical best fit parameters to describe the valve manufacturer's performance data reported as a function of C_V.

We used the following published correlations for estimation of adsorption equilibria (n^∞), LDF mass transfer coefficients (k), axial gas dispersion coefficient (D_L), and gas–solid heat transfer coefficient (h) which are input variables in the model.

Adsorption equilibria for pure N_2 on LiX zeolite (Rege and Yang 1997):

$$\begin{aligned} & n^\infty = \frac{KP}{1+BP}; \quad K = K^o \exp[Q_K/RT_s]; \\ & B = B^o \exp[Q_B/RT_s] \end{aligned} \tag{14}$$

Equation (14) is an empirical model for calculating pure gas equilibrium adsorption isotherms for N_2 on LiX zeolite at different temperatures. K and B are temperature dependent constants, and P is the gas pressure. The isosteric heat of adsorption of N_2 on the zeolite (Q_K) is 4.88 kcal/mole. The values of the model parameters can be found elsewhere (Rege and Yang 1997).

LDF mass transfer coefficient (k) for pure N_2 on zeolite (Ruthven 1984):

An order of magnitude of the lumped mass transfer coefficient (k) of Eq. (2) can be estimated by the following simplified model:

$$k = \frac{60D^e}{Kd_p^2}; \quad D^e = \frac{\varepsilon_p}{\tau_p}\left(\frac{1}{\frac{1}{D_k^e} + \frac{1}{D_m^e}}\right) \tag{15}$$

where D^e is the effective intra particle diffusivity of N_2 into the adsorbent particle. D_K^e and D_m^e are, respectively, the effective Knudsen and molecular diffusivity of N_2 into the adsorbent pore (Satterfield 1970; Kumar and Sircar 1986; Reid et al. 1977). ε_p and τ_p are, respectively, the pore void fraction and pore tortuosity. The temperature dependence of $D_K^e\left(\propto T^{0.5}\right)$ and temperature and pressure dependence of $D_m^e\left(\propto T^{1.5}/P\right)$ were included in the present work. K is the dimensionless Henry's law constant for N_2 adsorption on LiX zeolite at T (Rege and Yang 1997).

Equations (2) and (15) describe a simple but practical model of isothermal adsorbate mass transfer into a pelletized zeolite particle where the gas transport is controlled by diffusion through the binder pores and the adsorption isotherm is linear. Equation (2) is frequently used for PSA process simulations (Hufton and Sircar (2000)). Other complex kinetic models have also been proposed and reviewed, particularly for RPSA systems, by Todd and Webley (2006).

Mass axial dispersion coefficient (D_L) for N_2 (Ruthven 1984):

$$D_L = 0.7D_m^e + 0.5d_p Q/\left(\rho_g \bar{\varepsilon}\right) \tag{16}$$

Gas–solid heat transfer coefficient in presence of gas phase mass axial dispersion (Wakao et al. 1979):

$$\mathrm{Nu} = 2.0 + 1.1(Pr^{1/3}Re^{0.6}); \quad 15 \le \mathrm{Re} \le 8500 \tag{17}$$

The dimensionless parameters $Pr[= C_g\mu_g/k_g]$ and $Re\left[= d_pQ/\mu_g\right]$ in Eq. (17) are the gas phase Prandtl and Reynolds numbers, respectively. Equation (17) was used to estimate the gas–solid heat transfer coefficient (h) as

functions of d_p $\left[h = k_g Re\left(d_p, Q\right)/d_p\right]$ for a given gas mass flow rate (Q).

Dynamic mass balances:

The total specific amount (adsorbed + void gas) of N_2 [$\bar{n}(z,t)$, moles/kg] in the column at any z and t is given by:

$$\bar{n}(z,t) = n(z,t) + \varepsilon\left[\rho_g(z,t)/\rho_b\right] \tag{18}$$

The total specific amount (adsorbed + void) of N_2 in the column [$N(t)$] at time t during the pressurization or depressurization steps can be estimated by:

$$N(t) = \int_0^L \bar{n}(z,t)dz \tag{19}$$

The extent of completion (β) of the pressurization or depressurization process at time t is then given by the fraction.

$$\beta(t) = \frac{[N(t) - N(0)]}{[N^* - N(0)]} \tag{20}$$

where N^* is the total specific amount of N_2 in the column at the end (pressurization) and at the start (depressurization) of the processes. N (0) is the total specific amount of N_2 in the column at start of the pressurization process. Thus β varies from zero to unity and vice versa during the pressurization and depressurization processes, respectively. However, the times required for β to change from zero to unity vary depending on the conditions of operation.

The column is equilibrated with N_2 at P_{atm} and T^0 at the start of the pressurization process. This determines the value of $N(0)$. The column is equilibrated with N_2 at pressure $P^0$and temperature T^* at the end of the pressurization process and start of the depressurization process. The pressure of the inlet gas is held constant at P^0 during pressurization. The valve exit is maintained at ambient pressure during depressurization. The flow control valve sets the inlet and outlet flow of N_2 into and from the column.

3 Numerical simulations

The above described mathematical model for simulation of an adsorbent column pressurization and depressurization was solved using COMSOL Multiphysics with MATLAB which uses finite element analysis. Mesh densities of 240 spatial nodes and 300 time nodes were employed for the simulations. Using a workstation of Quad 2.93 GHz Intel Core i3 530 @3575 MB, the computation (CPU) time for simulation of a single pressurization-depressurization case varied between ~1–5 min, determined by the complexity of the case. Cases which included gas–solid heat transfer in the model often required long CPU times.

Four adsorber designs having different L/D ratios but containing the same total amount of adsorbent $[W = (\pi/4)D^2L\rho_b \sim 170\,\text{gms}]$ were used in the simulations. The L/D ratio was varied from 0.097 to 5.12 thus, covering conventional $(L/D > 2.5)$ to pancake $(L/D < 0.2)$ adsorber designs. The base case adsorber $(L/D = 2.5)$ consisted of $L = 12.7$ and $D = 5.0$ cm. The effects of (a) control valve C_V, (b) inlet N_2 pressure (P_0), and (c) adsorbent particle diameter (d_p) on the column pressurization and depressurization processes were evaluated and the influence of adsorption kinetics, column pressure drop, and gas phase axial mass and heat transfer dispersion on the duration of these processes were studied. The temperatures of the adsorbent at the start of the pressurization process and the inlet N_2 gas were equal to T_0. The simulations were carried out for a single successive pressurization–depressurization step and not for a cyclic process.

4 Simulation results

Figures 2–10 summarize the simulation results. The simulations were generally carried out for adiabatic columns using an inlet gas pressure of 4 atm and an adsorbent particle size of 400 μm (typical commercial LiX zeolite pellet diameter for RPSA application) while including all transport resistances listed earlier, unless stated otherwise. Each Figure plots β (t) as a function of time (t). The left and right hand plots of each figure, respectively, show the pressurization and depressurization characteristics.

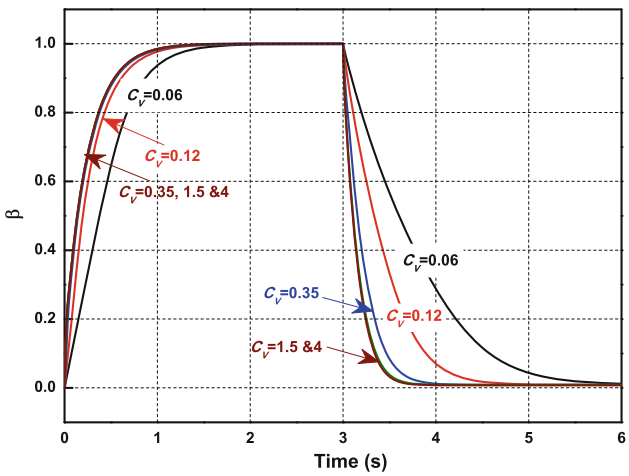

Fig. 2 Influence of C_V on column pressurization–depressurization times using $d_p = 400$ μm, $P^0 = 4$ atm

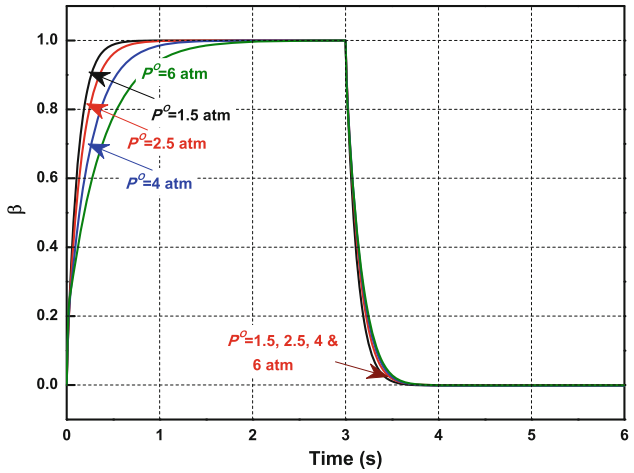

Fig. 3 Influence of inlet gas pressure (P^0) on column pressurization–depressurization times using $d_p = 400$ μm, $C_v = 4$

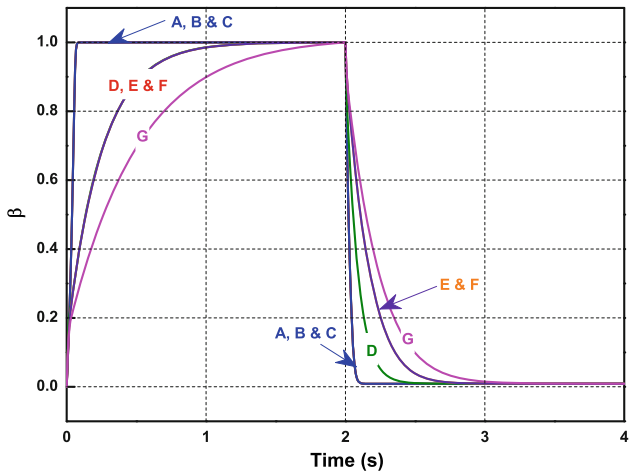

Fig. 4 Influence of various mass, heat and momentum transfer coefficients inside an adsorber column on pressurization–depressurization times using $C_V = 1.5$, $d_p = 400$ μm at $P^o = 4$ atm. *A*: Ideal, *B*: *A* + axial dispersion, *C*: *B* + heat dispersion, *D*: *C* + mass transfer kinetics ($k = 12$ s^{-1}), *E*: *D* + pressure drop, *F*: *E* + finite heat transfer; *G*:, *F* with $k = 6$ s^{-1}

4.1 Influence of valve constant (C_V)

Figure 2 shows that both pressurization and depressurization times increase as C_V of the inlet/outlet valve described by Fig. 1 is decreased, as expected. However, the depressurization times increase relatively more rapidly than the pressurization times with decreasing C_V. The Figure also shows that it is possible to carry out both steps in less than ~1 s if C_V is chosen to be >0.35 for the base case adsorber design. On the other hand, it may not be possible to carry out either of the steps in less than ~1.5 s if C_V is sufficiently low. The effect of increasing C_V on the pressurization–depressurization characteristics is minimal when $C_V > 1.5$. Consequently, we used a value of

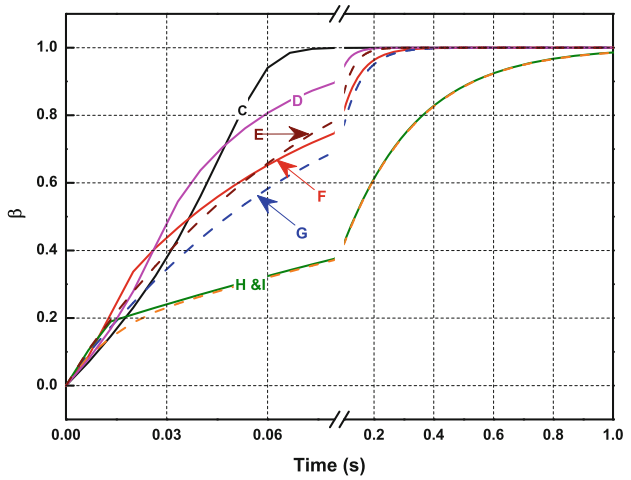

Fig. 5 Influence of column pressure drop on pressurization at early times using $C_V = 1.5$, $d_p = 400$ μm at $P^o = 4$ atm. *C*: ideal + gas dispersion + heat dispersion, *D*: *C* + mass transfer kinetics ($k = 96$ s^{-1}), *E*: *D* + pressure drop, *F*: *C* + mass transfer kinetics ($k = 48$ s^{-1}), *G*: *F* + pressure drop, *H*: *C* + mass transfer kinetics ($k = 12$ s^{-1}) and *I*: *H* + pressure drop. *Solid lines* are for without pressure drop model and *dash line* are for with pressure drop model

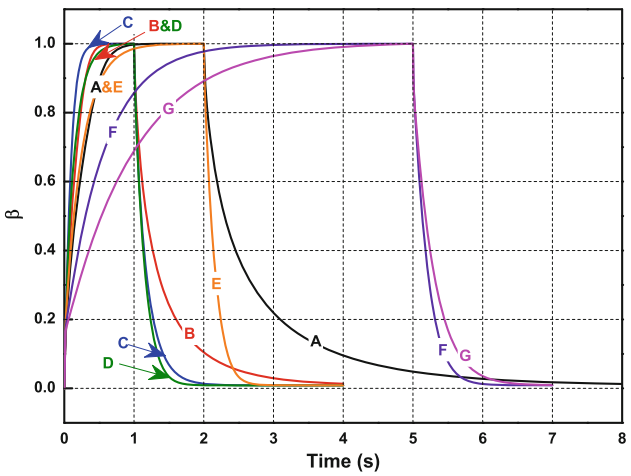

Fig. 6 Influence of adsorbent particle size (d_p) on column pressurization–depressurization times using $C_V = 4$ at $P^o = 4$ atm, $d_p = A$: 70 μm, *B*: 100 μm, *C*: 200 μm, *D*: 300 μm, *E*: 400 μm, *F*: 600 μm and *G*: 800 μm

$C_V > 1.5$ in order to eliminate the effect of valve flow constraint from all other simulation cases of this work.

4.2 Influence of inlet gas pressure (P^0)

Figure 3 shows the column pressurization–depressurization characteristics for different values of inlet gas pressures. It shows that increasing P^0 reduces the pressurization time, albeit by a small value while the depressurization time is practically independent of P^0 in the pressure range of the data even though the initial loading of the column at the

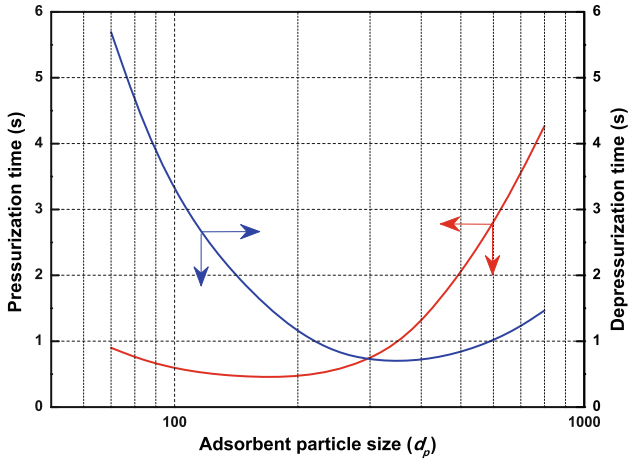

Fig. 7 Simulated base case pressurization–depressurization times as functions of adsorbent particle size

start of the depressurization step increases as P^0 is increased.

4.3 Effects of various mass, heat and momentum transfer resistances inside an adiabatic adsorber

Figure 4 demonstrates the effects of finite adsorbate mass transfer coefficient (k), gas–solid heat transfer coefficient, mass and heat transfer axial dispersion in the gas phase, and column pressure drop on the pressurization–depressurization characteristics. These were also generated using a C_V of 1.5 and an adsorbent particle size of 400 μm. The N_2 adsorption mass transfer coefficient for this particle size was estimated to be $\sim 12\ s^{-1}$ using Eq. (15).

Figure 4A corresponds to the ideal case where none of the transport resistances are present and instantaneous mass and thermal equilibrium is reached between the gas and solid. Figure 4B shows the case where only axial gas phase mass dispersion is added to the ideal case. Figure 4C shows the case where axial gas phase heat dispersion is also included. It may be seen that none of these non-idealities have significant effects on the pressurization–depressurization characteristics and they can be carried out well below 0.5 s. Figure 4D describes the case where the influence of adsorption kinetics ($k = 12\ s^{-1}$) is considered. It shows that adsorption kinetics appreciably stretches both times.

Figure 4E, F show the simulated cases where column pressure drop is added to the ideal case or to case 4D. They show that column pressure drop also stretches the pressurization–depressurization times from the ideal case. The effect of pressure drop is more pronounced for the depressurization process. Finally, Fig. 4G shows that the pressurization–depressurization times are significantly elongated for the case where a much slower adsorption kinetics ($k = 6\ s^{-1}$) exists. This figure also teaches that relatively slow adsorption kinetics may prevent operation of very rapid pressurization and depressurization steps.

4.4 Effect of column pressure drop

Figure 5 shows magnified plots of simulated β versus t profiles for various k values with and without column pressure drop in the early parts of the pressurization process. It shows that the effect of column pressure drop is complex. In general, the presence of column pressure drop slows down the pressurization process. The effect is more pronounced when the kinetics of adsorption is relatively faster.

4.5 Effect of particle size (d_p)

The simulated pressurization and depressurization characteristics for different adsorbent particle sizes ($d_p = 70$–800 μm, $C_V = 4$) are shown by Fig. 6. Smaller particle sizes offer larger adsorbate mass transfer coefficients (Eq. 15), but they also increase the column pressure drop (Eq. 5). Thus, there are two counteracting effects on the pressurization–depressurization times. It may be seen from Fig. 6 that both pressurization and depressurization times initially decrease when d_p is increased, reaching a relatively flat minimum, followed by an increase of both times at larger values of d_p. This complex behavior, which is caused by the differences in the degree of above-mentioned counter balancing effects in the pressurization and depressurization steps, is clearly demonstrated by Fig. 7 where these times are plotted as a function of d_p.

It may be seen from Fig. 7 that an over-all preferred adsorbent particle size of 200–350 μm may exist where both pressurization and depressurization times are relatively low (<1 s). It is very interesting to recall that a similar adsorbent particle size range was also found to be optimum for efficient N_2 desorption (lowest amount of O_2 purge quantity) from LiX zeolite by O_2 purge (Chai et al. 2012). That was also caused by differences in the complex interactive effects of column pressure drop and adsorption kinetics in an adiabatic column.

4.6 Influence of column *L/D*

The simulated effects of adsorber *L/D* ratio on the column pressurization and depressurization characteristics are shown by Fig. 8. In general, both pressurization and depressurization times are stretched when the *L/D* ratio is increased for a conventional adsorber design ($L/D > 2.5$). On the other hand, the effect of *L/D* ratio is reduced significantly in a pancake adsorber design ($L/D < 0.2$). For example, the figure shows that the pressurization and

depressurization characteristics for two pancake adsorbers ($L/D = \sim 0.1$ and 0.33) are nearly identical. The column pressurization and depressurization times can be drastically reduced by using pancake shaped adsorbers. Lowering L/D ratio (lowering L and increasing A) generally lowers column pressure drop. However, such adsorber designs can introduce other functional abnormalities like gas mal-distribution and particle agglomeration [Porter et al. (1993)].

4.7 Isothermal versus adiabatic pressurization–depressurization

Figure 9 compares the adiabatic (Fig. 9C, D) and isothermal (Fig. 9A, B) pressurization and depressurization characteristics for two values of adsorption mass transfer coefficients [$k = 12\ s^{-1}$ (Fig. 9A, C), and $k = 6\ s^{-1}$ (Fig. 9B, D)]. The figure shows that the adsorbate loading for the isothermal case is larger ($\beta > 1$) than that for adiabatic ($\beta = 1$) since $T^0 < T^*$, but the total times required for the pressurization and depressurization steps are close for both cases. For example, the times required for complete pressurization and depressurization steps are ~ 1.2 and 1 s, respectively, for both cases when $k = 12\ s^{-1}$.

4.8 Influence of ad(de) sorption mass transfer coefficient (k)

Obviously, the smaller is the value of the adsorbate mass transfer coefficient, the longer are the times required for the pressurization and depressurization processes as shown by Fig. 10. However, an important lesson from Fig. 10 is that fast (e.g. <1 s) pressurization or depressurization cannot be achieved if k is very small (<6 s^{-1}) under the conditions of this simulation. The pressurization and depressurization times are nearly as fast as those under local equilibrium conditions when $k > 100\ s^{-1}$.

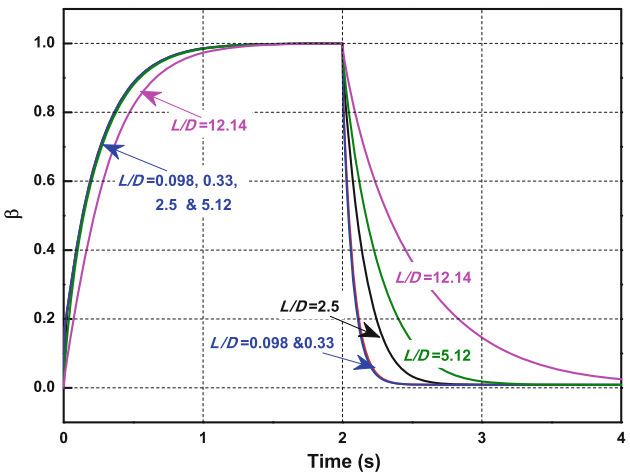

Fig. 8 Influence of column L/D on pressurization–depressurization times using $C_V = 4$, $d_p = 400$ μm, $P^0 = 4$ atm

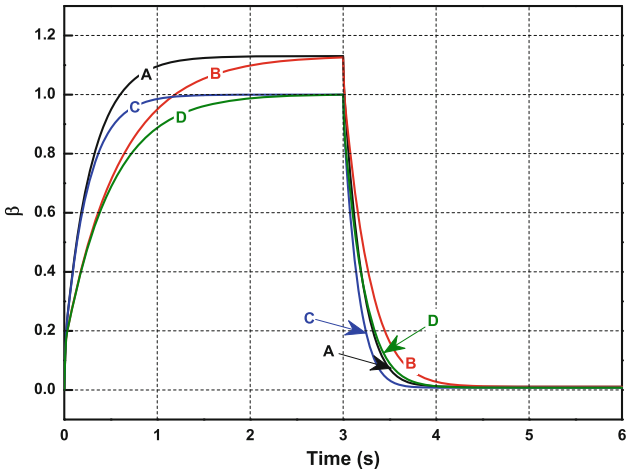

Fig. 9 Isothermal and adiabatic simulation of pressurization–depressurization using $C_V = 4$, $d_p = 400$ μm at $P^o = 4$ atm. *A*: Isothermal model ($k = 12\ s^{-1}$), *B*: Isothermal model ($k = 6\ s^{-1}$), *C*: Non-isothermal model ($k = 12\ s^{-1}$) and *D*: Non-isothermal model ($k = 6\ s^{-1}$)

4.9 Possible source of low k

The over-all value of k, according to Eq. 15, is controlled by molecular diffusion when the mean diameter of the binder pore (d, Å) is large. The Knudsen diffusion controls the value of k when d is small. Figure 11 gives a plot of k versus d for N_2 adsorption under the base case conditions of this work which shows that the value of k can easily vary between 1 and 13 s^{-1} over a plausible range of values of d (100 Å–10 μm).

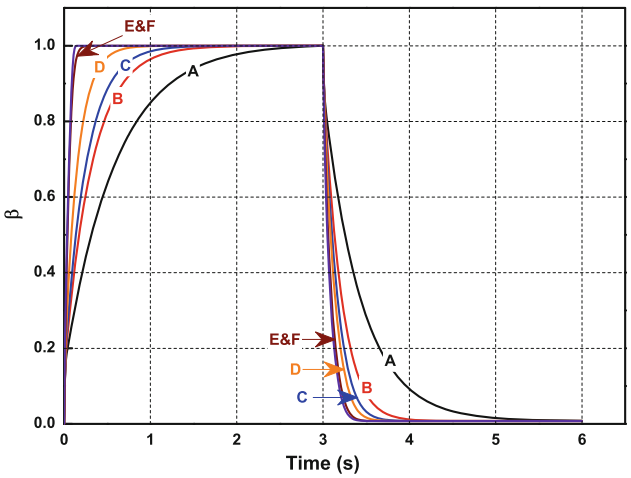

Fig. 10 Influence of mass transfer coefficient on pressurization–depressurization times using $C_V = 4$, $d_p = 400$ μm at $P^o = 4$ atm, *A*: $k = 2\ s^{-1}$, *B*: $k = 6\ s^{-1}$, *C*: $k = 12\ s^{-1}$, *D*: $k = 20\ s^{-1}$, *E*: $k = 100\ s^{-1}$ and *F*: $k = 1{,}440\ s^{-1}$

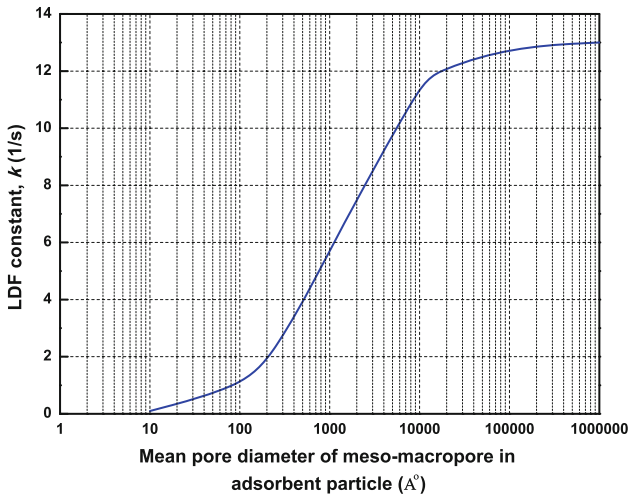

Fig. 11 Model estimation of k using Eq. 15 as functions of the mean meso-macropore diameter (d) in an adsorbent particle

5 Conclusions

The numerical simulation study indicates that rapid pressurization and depressurization times of less than a second for a LiX zeolite column can be achieved by using a large valve constant for the gas inlet/outlet control valve, a small adsorbent particle size, and a low column L/D ratio. Ad(de)sorption kinetics, column pressure drop, and column adiabaticity play major roles in establishing the pressurization–depressurization characteristics. Slower ad(de)sorption kinetics and column pressure drop stretch the pressurization–depressurization times. Axial dispersion of mass and heat through the gas phase inside the column, as well as a finite gas–solid heat transfer coefficient have small effects on the pressurization–depressurization processes. Smaller adsorbent particles increase ad(de)sorption kinetics but add to column pressure drop. These two counteractive effects cause both column pressurization–depressurization times versus particle size profiles to go through rather flat minimum values in the particle size ranges of 70–350, and 200–600 μm, respectively. The pressurization–depressurization times are reduced by lowering the column L/D ratio—the extent of reduction, however, becomes marginal for a pancake adsorber design ($L/D < 0.2$). The pressurization–depressurization times are qualitatively similar for isothermal and adiabatic processes for the system of current interest.

References

Chai, S.W., Kothare, M.V., Sircar, S.: Rapid pressure swing adsorption for reduction of bed size factor of a medical oxygen concentrator. Ind. Eng. Chem. Res. **50**, 8703 (2011)

Chai, S.W., Kothare, M.V., Sircar, S.: Numerical study of nitrogen desorption by rapid oxygen purge for a medical oxygen concentrator. Adsorption **18**, 87 (2012)

Chai, S.W., Kothare, M.V., Sircar, S.: Efficiency of nitrogen desorption from LiX zeolite by rapid oxygen purge in a pancake adsorber. AIChE J. **59**, 365 (2013)

Danckwerts, P.V.: Continuous flow systems, distribution of residence times. Chem. Eng. Sci. **2**, 1 (1953)

Ergun, S.: Fluid flow through packed columns. Chem. Eng. Prog. **48**, 89 (1952)

Hufton, J.R., Sircar, S.: Why does linear driving force model for adsorption kinetics work? Adsorption **6**, 137 (2000)

Jee, J.G., Lee, J.S., Lee, C.H.: Air separation by a small-scale two-bed medical oxygen pressure swing adsorption. Ind. Eng. Chem. Res. **40**, 3647 (2001)

Jee, J.G., Kim, M.B., Lee, C.H.: Pressure swing adsorption processes to purify oxygen using a carbon molecular sieve. Chem. Eng. Sci. **60**, 869 (2005)

Kumar, R., Sircar, S.: Skin resistance for adsorbate mass transfer into extruded adsorbent pellets. Chem. Eng. Sci. **41**, 2215 (1986)

Nikolic, D., Giovanoglou, A., Georgiadis, M.C., Kikkinides, E.: Generic modeling framework for gas separation using multi-bed pressure swing adsorption processes. Ind. Eng. Chem. Res. **47**, 3156 (2008)

Porter, K.E., Ali, Q.H., Hassan, A.O., Aryan, A.F.: Gas distribution in shallow packed beds. Ind. Eng. Chem. Res. **32**, 2408 (1993)

Rege, S.U., Yang, R.T.: Limits of air separation by adsorption with LiX zeolite. Ind. Eng. Chem. Res. **36**, 5358 (1997)

Reid, R.C., Prausnitz, J.M., Sherwood, T.K.: The properties of gases and liquids. McGrawhill, New York (1977)

Ruthven, D.M.: Principles of adsorption and adsorption processes. Wiley, New York (1984)

Santos, J.C., Cruz, P., Regala, T., Magalhaes, F.D., Mendes, A.: High purity oxygen production by pressure swing adsorption. Ind. Eng. Chem. Res. **46**, 591 (2007)

Satterfield, C.N.: Mass transfer in heterogeneous catalysis, pp. 72–76. M.I.T., Cambridge (1970)

Schiesser, W.E.: PDE boundary conditions from minimum reduction of the PDE. Appl. Numer. Math. **20**, 171 (1996)

Teague, K.G., Edgar, T.: Predictive dynamic model of a small pressure swing adsorption air separation unit. Ind. Eng. Chem. Res. **38**, 3761 (1999)

Todd, R.S., Webley, P.A.: Mass transfer models for rapid pressure swing simulation. AIChE J. **52**, 3126 (2006)

Wakao, N., Kaguei, S., Funazkri, T.: Effect of fluid dispersion coefficients on particle to fluid heat transfer coefficients in packed beds. Chem. Eng. Sci. **34**, 325 (1979)